# Energy Harvesting with Coupled Magnetorestrictive Resonators

## A NISE funded
## Basic Research Project

Suketu Naik
Visarath In
Alex Phipps

# SSC Pacific
## San Diego, California 92152-5001

**J. J. Beel, CAPT, USN**
**Commanding Officer**

**C. A. Keeney**
**Executive Director**

## ADMINISTRATIVE INFORMATION

Released by
K. S. Simonsen, Head
Advanced Concepts and
Applied Research Branch

Under authority of
M. J. Machniak, Head
Applied Sciences Division

Plexiglas® is a registered trademark of Rohm & Haas.

SB

# EXECUTIVE SUMMARY

In this report, we report the investigation of energy harvesting with coupled resonators while using magnetostrictive material called Galfenol. Galfenol is an alloy iron with an approximate concentration of iron and gallium as 83 and 17%, respectively. Here, we describe a coupled system of meso- scale (1- to 10-cm) cantilever beams. The coupled system can be used for harvesting vibration energy to power and aid the performance of low-power wireless sensor nodes.

The report is organized as follows. First we introduce the model of the transducer with Galfenol as the magnetostrictive material. Here, we discuss the model parameters derived from the experiment and show the simulations of a single beam. This is followed by the design of the power converters that are best suited for this device. Next, we analyze an all-to-all coupled system. Finally, we draw conclusions and describe the future course of the research.

# CONTENTS

# Figures

# Table

# ACRONYMS

| Acronym | Meaning |
|---------|---------|
| ADC | Analog-to-Digital Converter |
| CBM | Condition Based Maintenance |
| MCU | Micro Controller Unit |
| MEMS | MEMS |
| MsM | Magnetostrictive Material |
| PZT | Pb $[Zr_x Ti_{1-x}]$ $O_3$, $0<x<1$, Lead Zirconate Titanate |
| RX | Receiver |
| SHM | Structural Health Monitoring |
| Si | Silicon |
| SiN | Silicon Nitride |
| TX | Transmitter |
| UGS | Unattended Ground Sensors |
| UAV | Unmanned Aerial Vehicle |

# 1. INTRODUCTION

## 1.1 OBJECTIVES

Vibration energy harvested from ambient sources such as mechanical noise, wind, motion of aircraft, and ground vehicles can be a viable solution to extend mission lifetimes and enhance warfighter capabilities. The goal of this project is to develop a robust energy harvesting system consisting of coupled non-linear resonators with Galfenol as the magnetostrictive material at meso-scale (1 to 10 cm) and microscale (100 μm to 5 mm) and efficient power converters.

## 1.2 OPERATIONAL RELEVANCE

The proposed energy harvesting system can be used to power small-scale, low-power wireless electronic devices by gathering energy from mechanical vibrations in multiple application areas including unattended ground sensor (UGS) systems, unmanned aerial vehicles (UAVs), ground vehicles, small watercraft, human activity monitoring, communications, and health monitoring of the warfighter. Other uses include structural health monitoring (SHM) of bigger vessels and systems, and reduction of maintenance costs and an increase in safety for ships, aircraft, and machines.

## 1.3 BACKGROUND

At mesoscale, the dominant transduction mechanisms are electromagnetic and piezoelectric. The electromagnetic technique includes suspended magnets in a coil or a suspended coil in a magnet array that oscillates as it is excited with vibrational motion. These devices' performance rely heavily on the proximity of the magnets with the coil, strength of the magnets, and coil windings. For piezoelectric energy harvesting, materials that can integrate into standard processes have low coupling coefficients and more strongly coupled materials (e.g., lead zirconate titanate [PZT]) have lead in their fabrication process, which is an environmental risk.

Another major issue with standard energy harvesting techniques is that most transducers behave as second-order systems and are designed to have strong resonant behavior (i.e., high Q) to create more displacement. However, the amount of electrical energy produced is small for these devices when there is a mismatch between the resonant frequency of the device and the excitation frequency. The mismatch can be addressed by devices with non-linear resonance with extended bandwidth. Devices with non-linear springs can possibly perform better than a linear device, resulting in larger bandwidth under broadband random vibrations. Additionally, coupled systems of non-linear oscillators improve the performance of sensors by increasing sensitivity [1]. This concept can be used to harvest more energy by synchronization of individual energy harvesters in a coupled system.

The goal of this research is to develop coupled non-linear devices at mesoscale and microscale with Galfenol, which can be used for energy harvesting to power and aid the performance of a low-power wireless sensor node, as shown in Figure 1.

Wireless sensor nodes can be used in wireless sensor networks, which can enhance intelligence, surveillance, and reconnaissance (ISR) capability by (1) powering short-range, low-power wireless sensor networks, (2) autonomous monitoring of the physiological health of the warfighter (ECG/EEG signals), and (3) powering a sensor network for condition based maintenance (CBM) of shipboard machinery and SHM of ships, submarines, and UAVs.

In the first year of this project, the focus is on Galfenol-based coupled resonators at the meso-scale. A joint research effort at SPAWAR Systems Center Atlantic (SSC Atlantic) is focused on developing an efficient power conditioning circuit that can maximize the energy harvested under the

varying load conditions using both single and coupled devices. The power conditioning circuits will be used to charge solid-state batteries for energy storage.
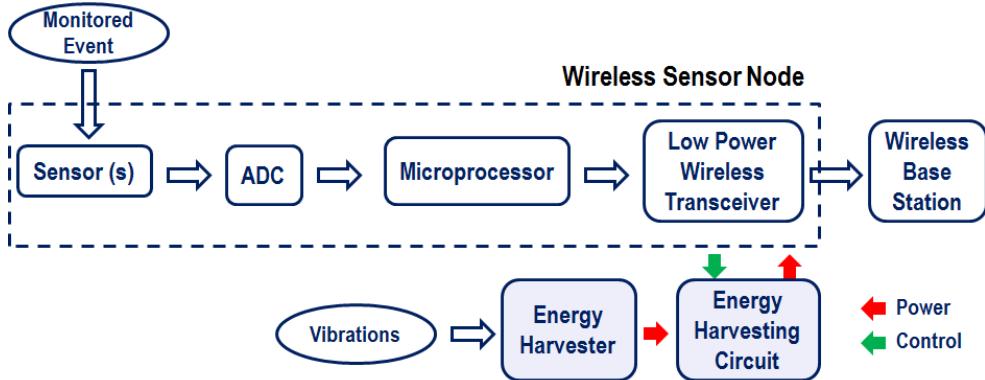


Figure 1. Magnetostrictive energy harvester and wireless sensor node.

### 1.3.1 Galfenol

Galfenol is a ferromagnetic material with a typical composition of $Fe_{83}Ga_{17}$. It is an MsM material and exhibits a large magnetostrictive affect: a 200- to 300-ppm strain at low applied magnetic field[1]. It has high-power generation and efficiency ($\sim 20$ mW/cm$^3$). Additionally, it exhibits low output impedance, which is good for matching, small hysteresis, and low coercivity[2]. Ceramic material like PZT tends to develop fatigue during its cycles whereas Galfenol does not have that issue because it behaves like metal. Its transduction efficiency is comparable to piezoelectric materials like PZT.[3]

# 2. SINGLE BEAM MODEL

To effectively design an efficient vibration energy harvesting system, it is first necessary to have an accurate model that captures the electromechanical behavior of the various system components (transducer, power electronics, and load) as well as their interaction to each other. In this section, a single beam model is first developed by using Galfenol samples from Etrema, Inc. These samples were nonstress-annealed and nonmagnetic field-annealed[4]. A non-linear model, based on the use of a non-linear spring constant, is also developed. Simulations using the non-linear spring model are discussed.

## 2.1 LINEAR TRANSDUCER MODEL

The experimental data were used to develop the combined linear transducer model. The test equipment included laser displacement sensors, a dynamical signal analyzer, and a shaker system, as

---

[1] T. Ueno. 2011. "Energy Harvester using Magnetostrictive Material (Galfenol)," Office of Naval Research (ONR) Galfenol Research Initiative Meeting, 2011. Contact S. Naik at SSC Pacific for availability of presentation.

[2] N. Lupu. 2011. "Fe-Ga Polycrystalline Materials: from Nanowires to Bulk Shaped Samples," ONR Galfenol Research Initiative Meeting, 2011. Contact S. Naik at SSC Pacific for availability of presentation.

[3] Ibid.

[4] Stress-annealing creates compressive stress in the material that is used for actuator application. Field-annealed samples tend to align magnetic domain perpendicular to the tension/compression direction of the beam and therefore provide better alignment while the beam is compressed as the domains rotate in the direction of tension/ compression. Field-annealed samples may yield better energy harvesting properties.

shown in Figure 2. A schematic of the magnetostrictive, mesoscale transducer explored in this work is shown in Figure 3. The transducer consists of an active Galfenol sample mounted onto a thin aluminum shim. This entire structure, both the shim and the Galfenol, is then wrapped with insulated magnet wire to form the coil.
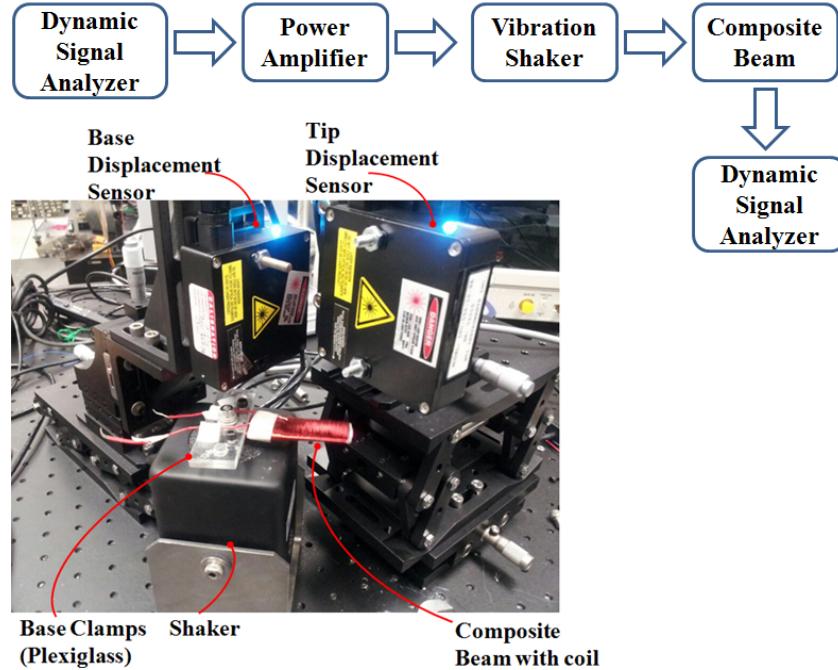


Figure 2. Block diagram of test setup and corresponding apparatus (partial).

As the base of the transducer is vibrated in the z-direction, inertial forces cause a relative displacement between the base and tip of the beam. The result of this displacement is a strain induced in the Galfenol in the x-direction, which generates a magnetic field (also in the x-direction) due to the magnetostrictive effect. Oscillations of the beam lead to a time-varying magnetic field within the coil, which produces a time-varying electrical current as a result of Faradaic induction.
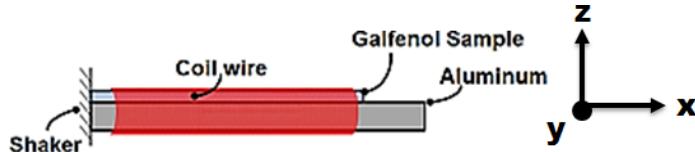


Figure 3. Cantilever beam with magnetostrictive energy harvesting transducer.

The linear transducer model used in this work is based on the principles of lumped element modeling, whereby the potential and kinetic energy distributed throughout the transducer beam is "lumped" together and assumed to occur at the tip of the beam. In this manner, the transducer can be modeled as a second-order mechanical system coupled to the electrical domain via the magneto-strictive effect and the electrical coil.

The mechanical domain of the transducer is represented by a second-order, mass-spring-damper system, as shown in Figure 4(a), where $M_m$ represents the lumped mass, $k_{ms}$ is the lumped spring constant, and $R_m$ is the lumped damping parameter. The effort variable is force, $F_m$, and the flow

3

variable is velocity, $V_m$. Since the transducer operates in both the electrical and mechanical domains, a more intuitive representation for this system is to use circuit elements to represent the lumped parameters, as shown in Figure 4(b).



(a)                                    (b)
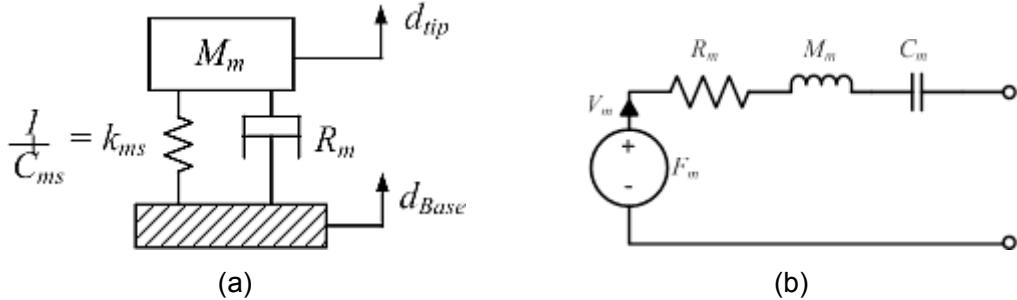
Figure 4. Mechanical domain lumped element model of the transducer beam shown with (a) mechanical components, and (b) electrical components.

The electrical domain of the transducer consists of the coil inductance, $L_{Coil}$, and its resistance, $R_{Coil}$, shown in Figure 5. The transduction between the two domains is modeled as a gyrator and shown in Figure 6 as a complete multiple domain model. Unlike the transformers commonly used in electrodynamic modeling, a gyrator assumes a linear relationship between the effort and flow variables of the two domains. For example, a linear relationship is assumed between the force in the mechanical domain and the current in the electrical domain. The gyrator transduction factor, K, lumps all of the energy transduction mechanisms (mechanical to magnetic to electrical) into a single term. The derivation of this term from first principles is not trivial, and was derived empirically for this work.
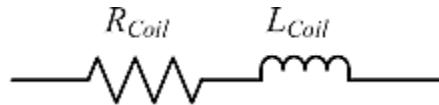


Figure 5. Lumped electrical domain model.
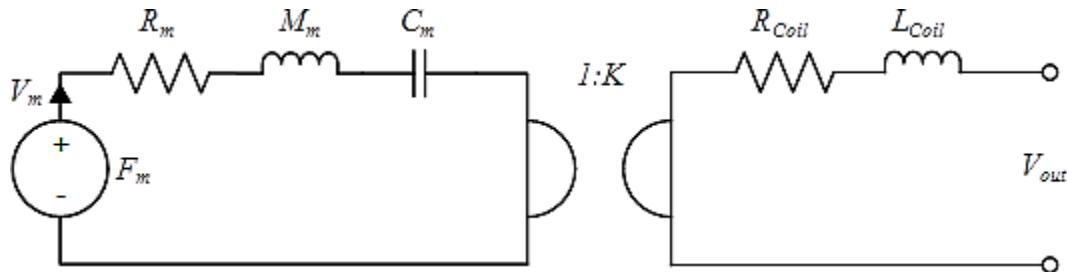


Figure 6. Full lumped element model with mechanical domain, electrical domain, and transduction.

## 2.2 EXTRACTION OF THE LINEAR TRANSDUCER PARAMETERS

To verify the accuracy of the linear model, various composite beams with Galfenol as the main material and with aluminum as the substrate were wrapped with a 35-gauge magnet wire for the coil. The beams were fitted to the test apparatus on top of the shaker using Plexiglas® or plastic plates to avoid interaction with the shaker magnet. The shaker was driven by an amplifier connected to the source of the dynamic signal analyzer, as shown in Figure 2. Some of the beams cracked and were

replaced during the testing. Various base clamping configurations and beam clamping methods were tried and an appropriate setup was created.

Figure 7(a) shows the frequency response curves measured on a dynamic signal analyzer. Here, base displacement and tip displacement were measured with laser sensors, and the output of the sensor was converted to the actual displacement values as shown in top and middle subfigures in Figure 7(a). The beam clearly shows non-linear behavior, i.e., soft-spring response. The resonance frequency shifts to the left as the vibration is increased. Here, the resonance peak shifts from 46.25 to 36.8 Hz. Soft-spring (non-linear) response occurs owing to the material compression-tension and the alignment of the magnetic poles while the beam is being vibrated. The non-linear behavior is crucial for the coupled system in which the non-linear behavior contributes to the synchronization of the individual beams and can potentially increase the output power.

The bottom subfigure in Figure 7(a) shows the output of the coil across a resistor that was matched to the coil resistance and the response shows an approximate peak value of 35.2 mV. Note that this value depends on the shaker vibration, the material, the base clamp configuration and beam structure.

The addition of the coil on top of the sample creates an imbalanced lumped mass that could contribute to the lowering of the effective mass. Additionally, the coil spreads the frequency response. In other words, the coil lowers the Q (based on the mechanical displacement amplitude vs. excitation frequency curve). As expected, when the frequency is swept up and down, a hysteresis was observed for a large vibration amplitude. The width of the hysteresis enlarges as the vibration amplitude increases. Figure 7(b) shows the normalized frequency responses of the tip, where the ratio of tip displacement relative to the base over the base acceleration is plotted. This ratio denotes the absolute tip displacement. Note that as the vibration amplitude is increased beyond a certain value, the normalized tip displacement drops down. This may be due to the non-ideal acceleration impinging on the tip of the beam as the base clamp and combined structure also contribute to additional vibration modes thereby reducing the tip displacement response. Note that this behavior can also occur due to beam breakage.

Experiments were conducted for the spring constant, mechanical to electrical transduction, and damping. The measured data of one of the beams was used to develop the linear and non-linear transducer model. Here, Figure 6 shows only the linear transducer model.

The shaker was vibrated at low amplitude to confine the vibration within linear regime, and the frequency response curves for the tip displacement and base displacement were used to determine the relative tip displacement ($Tip_{disp} - Base_{disp}$) over the base acceleration. The spring constant was measured using weight vs. displacement measurements and the resonance frequency was measured as 46.25 Hz. Using these values, the value of effective mass m or beam inductance $L_m$ in Figure 6 was determined. Using this value of effective mass as an approximation, the damping parameter b or beam resistance $R_m$ was derived using the Levenberg–Marquardt algorithm. The parameters for the coil were measured on the LCR meter, which measures inductance (L), capacitance (C), and resistance (R).

Two methods were used to determine the value of transduction factor K, from the mechanical side and from the electrical side. For the mechanical side measurement, the current output of the coil across a 10-MΩ resistor (open circuit) was measured for a given shaker vibration amplitude and corresponding tip velocity. Here, K = coil output voltage over tip velocity [V/ (m/s)]. Conversely, for the electrical side measurement, the coil was connected to the voltage source and the output vibration was measured, which was then converted to corresponding force. Here, K = tip force over input current [F/A]. The two values were close to each other and an average value was derived.
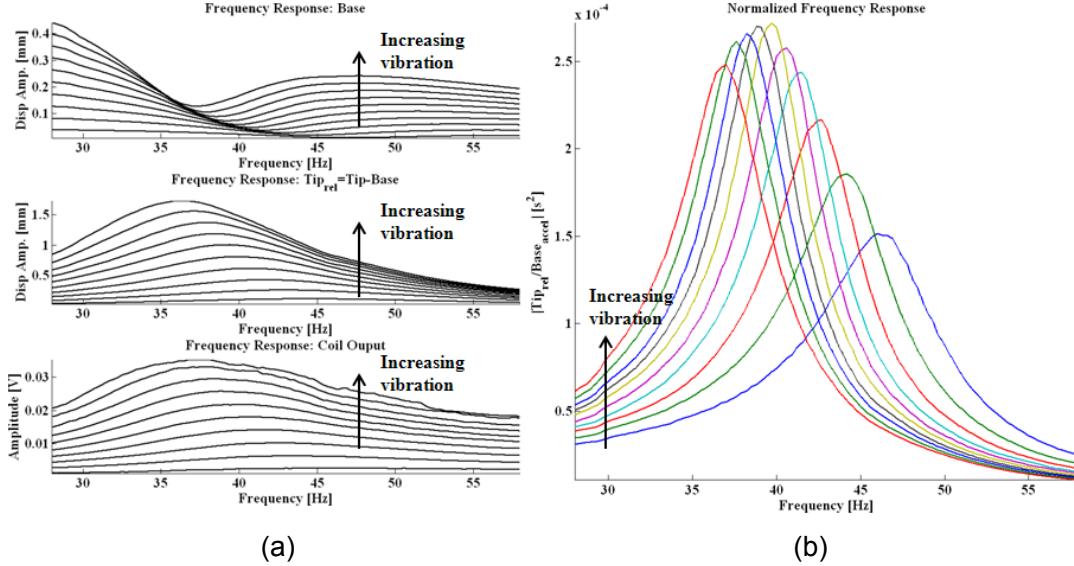
Figure 7. Frequency response curves of the composite fixed-free beam.

Table 1 lists the parameters mentioned in Figure 6 based on the estimation method described above.

Table 1. Measured and derived parameters for the model shown in Figure 6.

| Parameter | Symbol | Value | Unit |
|---|---|---|---|
| Beam Resonance Frequency | $f_o$ | 46.25 | Hz |
| Beam Capacitance | $C_m$ | 0.001758 | F |
| Beam Inductance | $L_m$ | 0.006734 | H |
| Beam Resistance | $R_m$ | 0.24 | $\Omega$ |
| Transduction Factor | K | 0.1448 | N/A or V/(m/s) |
| Coil Resistance | $R_{coil}$ | 198.58 | $\Omega$ |
| Coil Inductance | $L_{coil}$ | 47.16 | mH |
| Load | R | 180 | $\Omega$ |

**2.3 NON-LINEAR TRANSDUCER MODEL**

By using the other constants derived from the experiments, the simulations for the non-linear spring constant (numerical model with dynamical equations) were performed as shown in Figure 8.

Ideally, the soft potential behavior of the magnetic material would show up in the frequency response as hysteresis during up-sweep and down-sweep in the experiment. However, further increasing the base excitation to a higher amplitude (so that non-linearity is more prominent than damping) tends to break the beams. Both the measured and simulated responses show a distinct shift of the resonant frequency to the left and eventually a hysteresis shows up while increasing the excitation amplitude.

Here, the investigation and characterization of the non-linear resonance is important to assess (1) the widening of the excitation frequency range of a single beam, and (2) the properties of

6

synchronization of coupled beams. The experimental and simulated values of the non-linear spring constant do not match; however, the match is not critical for the simulation of the qualitative behavior for the coupled system (see Section 4).
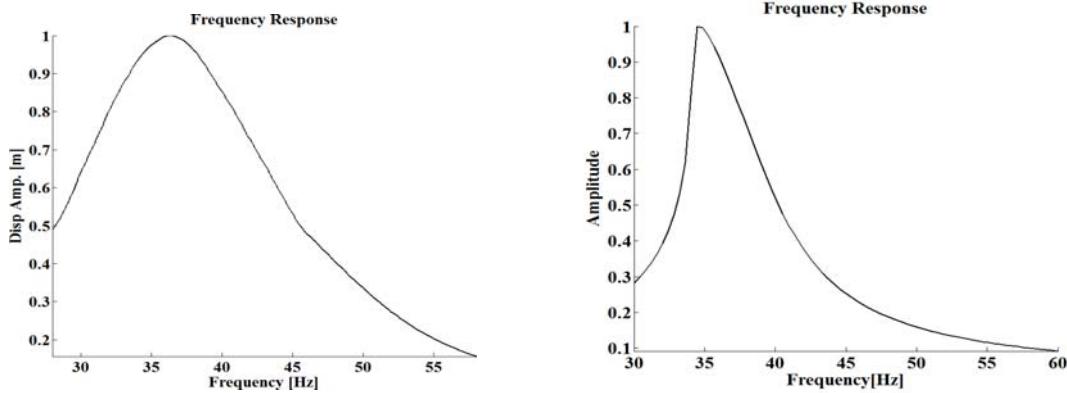


Figure 8. Frequency response of the non-linear transducer model: (a) measured frequency response with open load; (b) simulated frequency response based on dynamical equations.

# 3. DESIGN OF THE POWER CONVERTERS

The role of the power converter circuitry in the energy harvesting system is to provide rectification for the voltage signal generated by the transducer, as well as to enable maximum power transfer between the transducer and the electronic load or storage element (battery or capacitor). Since the amount of energy harvested is often lower than what is required to operate the electronic load (TX/RX, MCU, etc.), the use of a battery is critical to store enough energy to operate the load at a lower duty cycle. The inclusion of the rectification circuitry is necessary because the Galfenol beam generates AC voltage, and the battery requires a DC voltage. By simplifying the linear transducer model shown in Figure 6, a more direct analysis of the various power converter topologies can be performed.

In the same manner that electrical components on the primary side of a transformer can be reflected onto the secondary side, the mechanical components in Figure 6 can be reflected into the electrical domain. For reflection across a gyrator, components connected in series become connected in parallel, current sources become voltage source, and the impedance of inductors and capacitors are inverted (meaning that capacitors become inductors and vice-versa). A schematic view of the reflection of the mechanical domain into the electrical domain is shown in Figure 9, where the * corresponds to mechanical domain elements reflected into the mechanical domain.
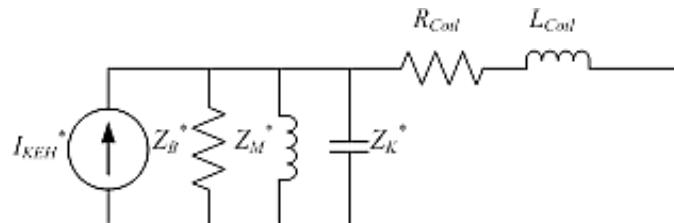


Figure 9. Simplified LEM of the beam driven at resonance.

For the LEM in Figure 9, which resides solely in the electrical domain, a further simplification can be made if it is assumed that this model is operating at its mechanical resonance frequency. This is a reasonable assumption, considering that cantilever beam transducers are resonant devices and will generate the largest amount of electrical power when excited at resonance. Assuming resonant operation, the contributions from the reactive components in the mechanical domain, $Z_M{}^*$ and $Z_K{}^*$, are equal and of opposite sign, and can be removed from the LEM, as shown in Figure 10.
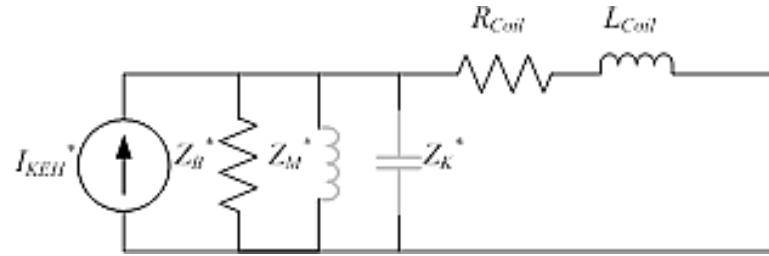


Figure 10. Schematic view of the transducer operating at mechanical resonance.

The next simplification to be made to the LEM is a Norton to Thevenin source transformation. In this case, the current source can be replaced by a voltage source, and the parallel resistance, Zb, is replaced by a series resistance, whose value is also $Z_B{}^*$. Since $Z_{BM}{}^*$ and $R_{Coil}$ are in series, they can be combined to give an effective resistance of $R_{KEH}$, as shown in Figure 11.
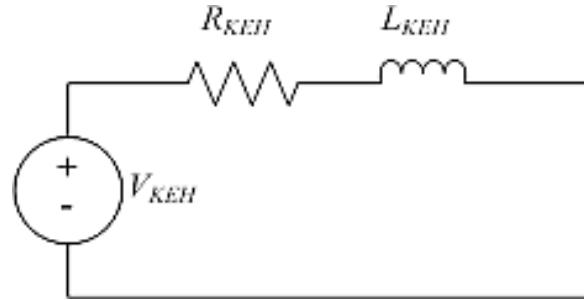


Figure 11. A simplified LEM of the beam driven at resonance.

Using fundamental power transfer theory, the optimal load for such a circuit would be a series resistor (of value $R_{KEH}$) and a series capacitor (with impedance of equal value to $L_{KEH}$ at the resonant frequency). However, such a load is not truly practical for harvesting energy since output voltage is AC, and not the steady DC required for charging a battery or operating electronic circuits.

A more useful circuit topology, shown Figure 12, includes a full-bridge rectifier that can deliver stable DC power to a load. While the goal of the power electronics circuit is to deliver power to a battery, a resistive load is a reasonable assumption for general system modeling. Power converter circuits used for battery charging, such as the flyback converter, can be modeled as resistive elements. Therefore, the power dissipated across the equivalent resistive load gives a reasonable approximation of the power that the flyback converter will deliver to a battery.

The pulsed resonant converter circuit in Figure 13 is based on the piezoelectric pulsed resonant circuit topology, which increases the power harvested by four times. Efforts are underway to determine if the pulsed resonant circuit topology will provide a similar increase in the harvested power for the magnetostrictive (piezomagnetic) type of transduction.
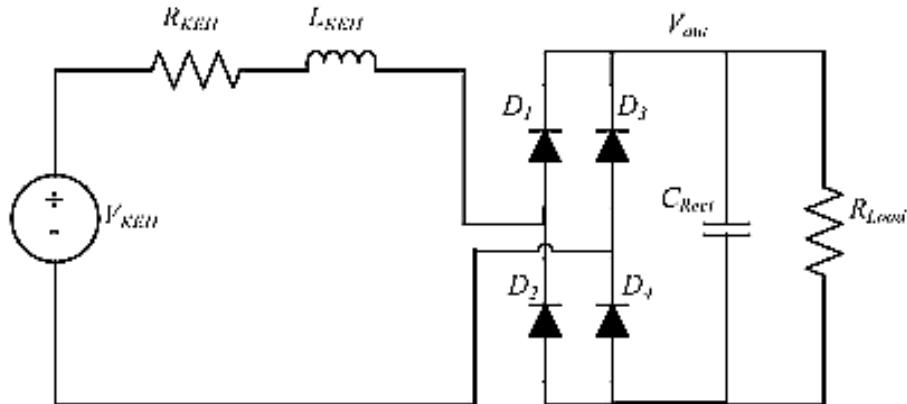
Figure 12. Resonant LEM model with rectifier and resistive load.
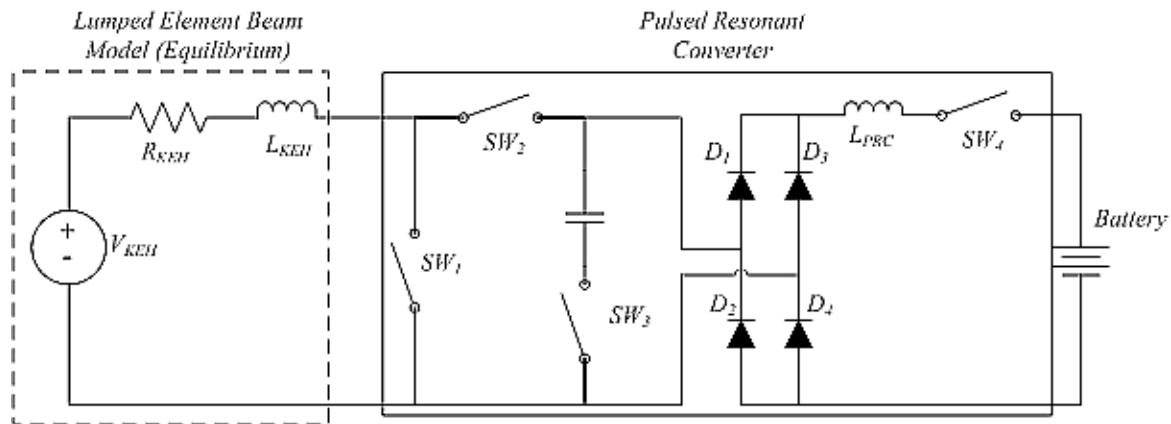


Figure 13. A pulsed resonant converter for inductive loads.

# 4. NUMERICAL SIMULATION OF COUPLED SYSTEM

In this section, we briefly show the results of numerical simulation of the coupled system with three resonators.

## 4.1 DERIVATION OF COUPLING CONSTANTS

Initial experiments on the coupled beams were conducted to approximate the coupling constants. Two types of coupling exist between the beams: (1) vibrational coupling through the base, and (2) mutual inductance between the beams through read-out coils. Here, vibrational coupling can be estimated as the average of the proportional displacements of the two beams while uncoupled and coupled. Vibrational coupling depends on position of the beams on the base, the clamp holes, and clamp screw strengths (which relates to damping), and the mass/coil variation between the beams. Mutual inductance was not observable in the experiment. This may be due to the small amplitude of the magnetic field generated in the beams. Note that the mutual inductance value will depend on the vibrational coupling between the beams as well as the distance between the beams. To simplify the coupling mechanism, we assume vibrational coupling only.

## 4.2 ALL-TO-ALL COUPLED SYSTEM[5]

Research by team members on coupled systems of non-linear resonators/oscillators shows that the sensitivity of the system increases greatly at the bifurcation boundary [1] [2]. Here, we would exploit this property to explore and enhance energy harvesting property of the coupled system. Both chain and ring coupled systems are being investigated. While the chain configuration may represent a specific case of the ring configuration, our research will focus on analyzing and maximizing the power output of the coupled system of Galfenol beams regardless of the type of configuration.

For N number of resonators in a ring configuration with resistive-capacitive load, the dynamical equations of $j^{th}$ resonator can be written as follows:

$$m\ddot{z}_j(t) + b\dot{z}_j(t) + k_1 z_j(t) + k_3 z_j(t)^3 + G i_T + \lambda \Omega_j = A_d \cos(\omega_d t) \tag{1}$$

$$L_c C_s \ddot{V}_j(t) = G\dot{z}_j(t) - C_s(R_L + R_c)\dot{V}_j(t) - V_j(t) \tag{2}$$

where, $m$ = mass of the resonator [kg] = $L_m$ in Table 1,

$b$ = damping parameter [N*s/m] = $R_m$ in Table 1,

$k_1$ = linear spring constant [N/m] = $1/C_m$ in Table 1, $k_3$ = non-linear spring constant [N/m$^3$],

$G$ = transduction factor [N/A] = K in Table 1, $\lambda$ = vibrational coupling constant [N/m],

$\Omega$ = coupling function = $Z_1 + Z_2 + Z_3$ = all-to-all coupling or sum [m] with $S_3$ symmetry [3],

$A_d$ = excitation amplitude [N], $\omega_d$ = excitation frequency [rad],

$L_c$ = read-out coil inductance [H], $C_s$ = load capacitance [F], $R_L$ = load resistance [ohm],

V = output voltage [V], Z = displacement in z-direction [m]

Next, we define the dimensionless variables and parameters as

$$\tau = \omega_0, z_j(t) = \sqrt{\frac{k_1}{|k_3|}} x_j(\tau), \tag{3}$$

$$\frac{d}{dt}(z_j(t)) = \omega_o \sqrt{\frac{k_1}{|k_3|}} \frac{d}{d\tau}(x_j(\tau)), \tag{4}$$

$$\frac{d^2}{dt}(z_j(t)) = \omega_o{}^2 \sqrt{\frac{k_1}{|k_3|}} \frac{d^2}{d\tau}(x_j(\tau)), \tag{5}$$

Let,

$$V_j(t) = \frac{k_1}{C_s \omega_o G} \sqrt{\frac{k_1}{|k_3|}} U_j(\tau), \tag{6}$$

$$\frac{d}{dt}(V_j(t)) = \frac{k_1}{C_s G} \sqrt{\frac{k_1}{|k_3|}} \frac{d}{d\tau}(U_j(\tau)), \tag{7}$$

$$\frac{d^2}{dt}(V_j(t)) = \frac{k_1}{C_s G} \sqrt{\frac{k_1}{|k_3|}} \frac{d^2}{d\tau}(U_j(\tau)). \tag{8}$$

---

Noting that (′) and (″) denote first and second derivatives with respect to $\tau$, we re-write the Equations (1) and (2) in dimensionless form by using Equations (3) through (8) as follows:

$$x_j''(\tau) + \frac{1}{Q}x_j'(\tau) + x_j(\tau) + \gamma x_j(\tau)^3 + U_j'(\tau) + \lambda_r \Omega_{rj} = F_r \cos(\omega_r \tau), \tag{9}$$

$$U_j''(\tau) = k^2 x_j'(t) - \frac{1}{\alpha}U_j'(\tau) - \frac{1}{L_c C_s \omega_o^2}U_j(\tau), \tag{10}$$

where,

$$\lambda_r = \frac{\lambda}{k_1}, k^2 = \frac{G^2}{L_c k_1}, \gamma = sgn(k_3), F_r = \frac{\sqrt{|k_3|}}{G^{3/2}}A_d, \omega_r = \frac{\omega_d}{\omega_o}, \alpha = \frac{L_c \omega_o}{(R_L + R_C)}. \tag{11}$$

Here, we assume that the coil generates sufficient current through the magnetostrictive property of Galfenol to charge the load capacitor. Also, note that the dimensionless Equations (9) and (10) are valid for the coupled system at meso-scale as well as micro-scale.

## 4.4 BIFURCATION DIAGRAM

Bifurcation diagrams for three energy harvesters in ring configuration were obtained using software package AUTO. Here, we focus in two coupling regimes, weak and strong. As a convention, solid/dashed lines and filled-in/empty circles corresponding to stable/unstable equilibrium points and stable/unstable periodic solutions, respectively, in the Figure 14.

As shown in Figure 14(a), the resonator exhibits pitchfork bifurcation when it is not forced. Here, for coupling constant values less than a critical value (shown by rectangular box), the system shows unstable fixed point after which one stable fixed and two unstable fixed points appear through pitchfork bifurcation.

As shown in Fig. 1(b), the system first exhibits unstable solutions as coupling constant is swept from -1 to 1. These solutions form stable solutions at a certain $\lambda_r$, where the resonators exhibit travelling wave pattern with zero mean and two resonators completely synchronize with each other. These regions are indicated by branch 2 and 3 in Figure 14(b). Here, it is interesting to note that for both weak and strong coupling constant values, the system exhibits full synchronization, which is indicated by branch 1 in Figure 14(b).
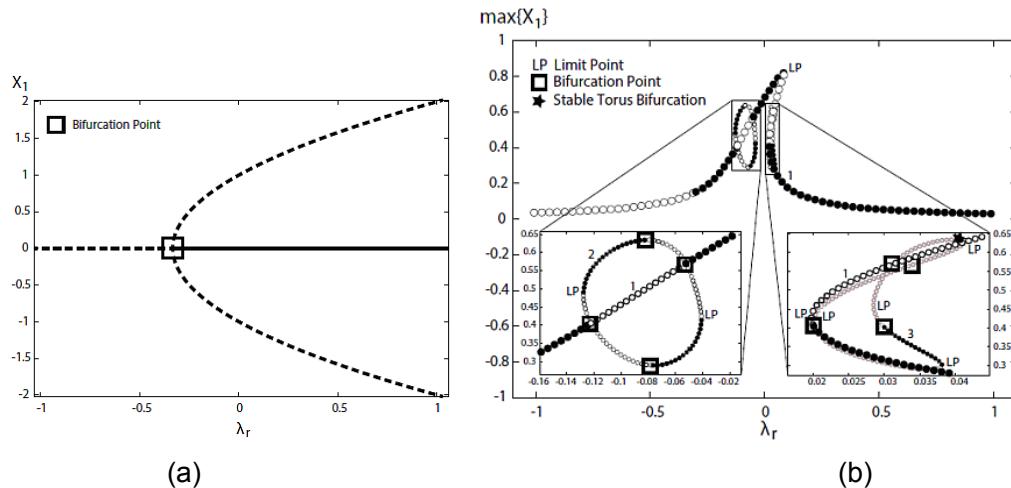


Figure 14. Bifurcation diagrams with $\lambda_r$ as the bifurcation parameter for one of the resonators within N = 3 coupled system: (a) no forcing with $F_r$ = 0 and (b) periodic forcing with $F_r$ = 0.1. Here, the solid lines and filled dots represent stable fixed points and stable periodic solutions, respectively. Note that $\omega_r$ = 0.9, Q = 100, $\alpha$ = 1, $k^2$ = 0.2, and $\gamma$ = -1, $1/(L_c C_s \omega_o^2)$ = 0.1.

The system shows that rich dynamical behavior and multiple bifurcations occur, through which the system enters partial and fully synchronized states. We are currently investigating several cases, including (1) the role of mutual coupling along with the vibrational coupling, (2) bidirectional coupling, and (3) the effect of the broadband excitation signal.

# 5. CONCLUSIONS AND FUTURE WORK

This section concludes the key points of the research and entails the direction of the future work.

## 5.1 CONCLUSIONS

1. With a single sample (1.5-cm wide x 7.5-cm long x 0.5-mm thin) on Al substrate, the maximum observed power was 2.5 uW at 1-g acceleration and 40 Hz (SSC Pacific measurement).

2. With a stack of four samples (1.5-cm wide x 7.5-cm long x 0.5-mm thin) with bias magnets and a low permeability yoke, the maximum observed power was 800 uW at 1-g acceleration and 42 Hz and 1.7 mW at 1-g acceleration at 120 Hz (SSC Atlantic measurement). Here, we note that the bias magnets and stacking more samples increases the power significantly.

3. We assessed pulsed resonant power converter, which needs to be modified for the coupled system of energy harvesters to address phase difference between the signals.

4. Development of linear and non-linear transducer models based on experimental data was conducted.

5. We also analyzed the coupled system with three resonators and performed numerical simulations to understand the synchronization behavior for weak and strong vibrational coupling constants.

6. Experiments on various types of beams are ongoing. One type of device includes the beam as a composite of Galfenol samples and aluminum substrate wrapped with a thin and small gage wire (shown in Figure 2). The other test setup includes a Galfenol sample without any substrate and a planar coil on top. This setup emulates the microscale version of the beam (for future investigation) at mesoscale qualitatively. Here, we observed a hard-spring effect as the excitation amplitude increases. In addition, the peak shifts to the left at low excitation. The peak power was 250 nW at 1 g at 35 Hz.

## 5.2 FUTURE WORK

1. Coupled system experiments: we would like to observe any noticeable increase in power and scaling law (output power vs. number of resonators) as N becomes larger. Additionally, these experiments will also reveal the advantage of coupled beams over single beams, if any.

2. Power converters: we would like to simulate and analyze both out-of-phase and in-phase output signal designs for the coupled system.

3. Coupled system simulations: while continuing the numerical simulation, we would like to investigate coupled system with a large number of resonators. This would allow the properties of synchronization and show how scaling law changes from small N system.

4. Integration with wireless sensor node: we would like to assess the performance of the coupled system at mesoscale for powering the wireless sensor node.

5. Microscale implementation: we would like to shift our focus on the analyses, design, and characterization of coupled energy harvesters on Si or SiN substrate with a thin film deposition of Galfenol at microscale. This work will allow the miniaturization of the devices and, hence,

autonomous monitoring of various signals and events in an unattended sensor network. Here, the microscale harvesters can be integrated with sensors to power them and/or aid their performance.

6. One of the future goals includeu using the coupled system in a hybrid system that can harvest energy from multiple sources such as light, heat, and vibration and convert it into useful electrical power.

# 6. REFERENCES

[1] V. In, A. R. Bulsara, A. Palacios, P. Longhini, A. Kho, and J.'D. Neff. 2003. "Coupling Induced Oscillations in Overdamped Bistable Systems," *Physical Review E*, vol. 68, no. 4, pp. 045102–1:045102–4.

[2] S. Naik, T. Hikihara, H. Vu, A. Palacios, V. In, and P. Longhini. 2012. "Local Bifurcations of Synchronization in Self-excited and Forced Unidirectionally Coupled Micromechanical Resonators," *Journal of Sound and Vibration*, vol. 331, no. 5, pp. 1127–1142.

[3] M. Golubitsky, I. Streward, and D. Schaeffer. 1988. *Singularity and Groups in Bifurcation Theory: Vol II*, J. E. Marsden and L. Sirovich, Eds. Springer-Verlag New York, Inc., New York, NY.

# 7. BIBLIOGRAPHY

G. Sebald, H. Kuwato, D. Guyomar, and B. Ducharne. 2011. "Simulation of a Duffing Oscillator for Broadband Piezoelectric Energy Harvesting," *Smart Materials and Stru*ctures, vol. 20, no. 075022, pp. 075022:1–17.

L. Wang and F.G. Yuan. 2006. "Structural Vibration Energy Harvesting by Magnetostrictive Materials (MsM)." *Proceedings of 4th China-Japan-US Symposium on Structural Control and Monitoring* (pp. 147–152), October 16–17, Hangzhou, China.

# REPORT DOCUMENTATION PAGE

| 1. REPORT DATE *(DD-MM-YYYY)*<br>September 2013 | 2. REPORT TYPE<br>Final | 3. DATES COVERED *(From - To)* |
|---|---|---|

| 4. TITLE AND SUBTITLE<br><br>Energy Harvesting with Coupled Magnetostrictive Resonators<br><br>A NISE funded Basic Research Project | 5a. CONTRACT NUMBER |
|---|---|
| | 5b. GRANT NUMBER |
| | 5c. PROGRAM ELEMENT NUMBER |
| 6. AUTHORS<br><br>Suketu Naik<br>Visarath In<br>Alex Phipps | 5d. PROJECT NUMBER |
| | 5e. TASK NUMBER |
| | 5f. WORK UNIT NUMBER |

| 7. PERFORMING ORGANIZATION NAME(S) AND ADDRESS(ES)<br><br>SSC Pacific, 53560 Hull Street, San Diego, CA 92152–5001 | 8. PERFORMING ORGANIZATION REPORT NUMBER<br><br>TR 2024 |
|---|---|

| 9. SPONSORING/MONITORING AGENCY NAME(S) AND ADDRESS(ES)<br>Office of Naval Research<br>Naval Innovation Science and Engineering (NISE) Program<br>One Liberty Center<br>875 N. Randolph Street, Suite 1425<br>Arlington, VA 22203-1995 | 10. SPONSOR/MONITOR'S ACRONYM(S)<br>ONR NISE |
|---|---|
| | 11. SPONSOR/MONITOR'S REPORT NUMBER(S) |

**12. DISTRIBUTION/AVAILABILITY STATEMENT**

Approved for public release.

**13. SUPPLEMENTARY NOTES**

This is work of the United States Government and therefore is not copyrighted. This work may be copied and disseminated without restriction.

**14. ABSTRACT**

In this report, we report the investigation of energy harvesting with coupled resonators while using magnetostrictive material called Galfenol. Galfenol is an alloy iron with an approximate concentration of iron and gallium as 83 and 17%, respectively. Here, we describe a coupled system of mesoscale (1- to 10-cm) cantilever beams. The coupled system can be used for harvesting vibration energy to power and aid the performance of low-power wireless sensor nodes.

The report is organized as follows. First we introduce the model of the transducer with Galfenol as the magnetostrictive material. Here, we discuss the model parameters derived from the experiment and show the simulations of a single beam. This is followed by the design of the power converters that are best suited for this device. Next, we analyze an all-to-all coupled system. Finally, we draw conclusions and describe the future course of the research.

**15. SUBJECT TERMS**

| | | | |
|---|---|---|---|
| Galfenol | non-linear transducer | energy harvesting | magnetostrictive resonators |
| Linear transducer | coupling constants | lumped element model | unattended ground sensors |

| 16. SECURITY CLASSIFICATION OF: | | | 17. LIMITATION OF ABSTRACT | 18. NUMBER OF PAGES | 19a. NAME OF RESPONSIBLE PERSON<br>Suketu Naik |
|---|---|---|---|---|---|
| a. REPORT | b. ABSTRACT | c. THIS PAGE | | | |
| U | U | U | U | 21 | 19B. TELEPHONE NUMBER *(Include area code)*<br>(619) 767-4339 |

# INITIAL DISTRIBUTION

Approved for public release.



SSC Pacific
San Diego, CA 92152-5001